

Deep Learning-based End-to-end Diagnosis System for Avascular Necrosis of Femoral Head

Yang Li*, Yan Li*, Hua Tian

Abstract—As the first diagnostic imaging modality of avascular necrosis of the femoral head (AVNFH), accurately staging AVNFH from a plain radiograph is critical and challenging for orthopedists. Thus, we propose a deep learning-based AVNFH diagnosis system (AVN-net). The proposed AVN-net reads plain radiographs of the pelvis, conducts diagnosis, and visualizes results automatically. Deep convolutional neural networks are trained to provide an end-to-end diagnosis solution, covering femoral head detection, exam-view/sides identification, AVNFH diagnosis, and key clinical note generation subtasks. AVN-net is able to obtain state-of-the-art testing AUC of 0.95 (95% CI: 0.92 – 0.98) in AVNFH detection and significantly greater F1 scores ($p < 0.01$) than less-to-moderately experienced orthopedists in all diagnostic tests. Furthermore, two real-world pilot studies were conducted for diagnosis support and education assistance, respectively, to assess the utility of AVN-net. The experimental results are promising. With the AVN-net diagnosis as a reference, the diagnostic accuracy and consistency of all orthopedists considerably improved while requiring only 1/4 of the time. Students self-studying the AVNFH diagnosis using AVN-net can learn better and faster than the control group. To the best of our knowledge, this study is the first research on the prospective use of a deep learning-based diagnosis system for AVNFH by conducting two pilot studies representing real-world application scenarios. We have demonstrated that the proposed AVN-net achieves expert-level AVNFH diagnosis performance, provides efficient support in clinical decision-making, and effectively passes clinical experience to students.

Index Terms—Avascular necrosis of the femoral head, clinical decision-making, deep convolutional neural network, diagnosis, education assistance, radiography.

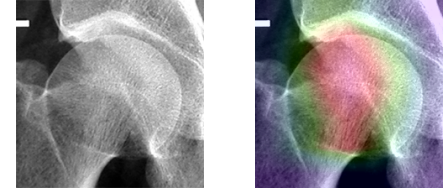
I. INTRODUCTION

AVASCULAR necrosis of the femoral head (AVNFH) is characterized as progressive pain and disabling degeneration of the hip joint that typically affects the active, middle-aged population (30-50 years) [1][2]. In the United States alone, approximately 20,000 to 30,000 new AVNFH patients are diagnosed annually [3], and a high probability of bilateral involvement (73%) has been reported previously [4]. Note that early presentation of AVNFH is typically asymptomatic and painless [5]. However, over 70% of asymptomatic cases can transform to symptomatic and femoral head (FH) collapse which ultimately requires hip arthroplasty [6][7][8]. The mean interval between the first symptoms and the FH collapse is only 12 months [6]. Although there is no consensus on the

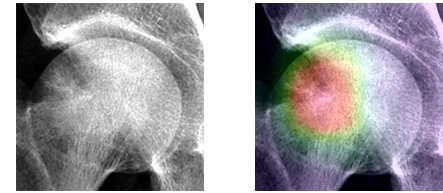
*Equal contributions.

Yang Li (email: liyangdr@bjmu.edu.cn) and Hua Tian (email: tianhua@bjmu.edu.cn) are with the Orthopedics Department of Peking University Third Hospital, Beijing, 100191, China

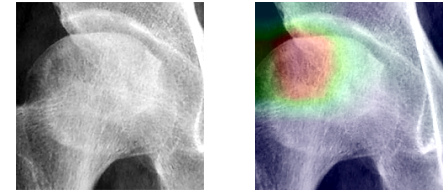
Yan Li is with the Department of Electrical & Computer Engineering, University of Toronto, 10 King's College Rd, Toronto, ON M5S 3G4, Canada. (email: yyaann.li@mail.utoronto.ca)



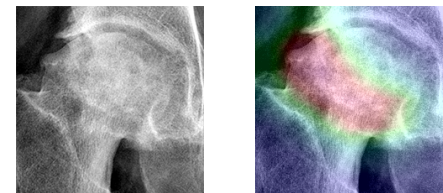
(a) AVNFH absence: No findings



(b) AVNFH stage II: Sclerotic and cystic changes



(c) AVNFH stage III: Subchondral collapse



(d) AVNFH stage IV: FH and acetabular deformation

Fig. 1: Examples of different AVNFH stages (left), visualized diagnosis (right), and generated clinical notes (captions).

etiology of AVNFH, a range of traumatic and atraumatic risk factors have been identified; thus, various interventions have been developed to alleviate the pain and delay progression [2][3][5]. However, the success of treatments is highly dependent on the stage at which care is initiated [1]. Therefore, timely and accurate staging is essential to optimizing AVNFH treatments, especially for early-stage cases.

Clinically, the first imaging modality for AVNFH diagnosis is radiography due to its cost, accessibility, and efficiency advantages. Radiographs from both anteroposterior (AP) and frog-leg lateral (FL) views are typically required to obtain a comprehensive diagnosis because they contain complementary areas of the hip joint [1]. The Ficat staging system, a

widely used AVNFH diagnosis standard based on radiographs, provides practical guidance for classifying AVNFH into five stages with severity increasing from stage 0 (normal imaging) to stage IV (FH and acetabular deformation) [9]. However, the modest changes in the early stage of AVNFH (Fig. 1) poses significant challenges to diagnostic sensitivity [10], which results in low inter-/intra-reader agreements [11]. As a result, clinicians typically require years of training and practice to perform accurate diagnoses.

With rapid advancements in deep learning (DL) methodologies, deep convolutional neural networks (DCNN) have demonstrated exceptional capabilities in solving disease diagnosis problems. Using annotated data, some DCNN algorithms have reached the performance of human experts in various diagnostic tasks, e.g., in ophthalmology [12][13], dermatology [14][15], and orthopedics [16][17] fields. Unfortunately, only a small number of studies have attempted to approach AVNFH diagnosis by leveraging DL methodologies which possibly because of two reasons. First, there is no publicly available dataset with high quality of annotations for AVNFH diagnosis. More importantly, the nature of AVNFH poses a number of challenges to DL algorithms and hence makes this task more difficult. In particular, the lesion of AVNFH is highly localized; thus, the majority proportion of the information on a pelvic radiograph would be irrelevant to diagnostic decision-making. To improve the performance of the DL model, it is common to manually crop the region-of-interest (ROI) from a radiograph before training. However, this process inevitably complicates the data preparation and impedes the application of the DL model. In addition, in most studies of DL in medicine, discussions typically stop at performance comparisons between algorithms and experts. No further analysis has been provided to demonstrate how well DL models perform in real-world scenarios.

To address these issues, we propose the AVN-net, a fully automated AVNFH diagnosis system based on DCNNs and plain radiographs of the pelvis. AVN-net comprises five functional modules to perform the FH detection, exam view identification, side classification, AVNFH diagnosis, and key clinical note generation subtasks in an end-to-end fashion. The FH detection module extracts the ROI (i.e., the FH) from the input radiograph. Then, four downstream modules are trained using the detected FH data to perform the remaining tasks. Experimental results demonstrate that the proposed AVN-net can achieve state-of-the-art testing performance and significantly outperforms less-to-moderately experienced orthopedists.

We performed two pilot studies to investigate the utility of AVN-net in real-world application scenarios. In the first study, AVN-net was used to provide orthopedists with a “second opinion” in AVNFH staging. Here we compared the diagnostic performance and time consumption of orthopedists with and without AVN-net to assess its effectiveness in supporting clinical decision making. In the second study, AVN-net was applied as an experienced teaching assistant to help medical students self-learn AVNFH diagnosis because we believe the quality of self-study plays a critical role in medical education due to increasingly limited educational resources. We tested the performance of two groups of students (i.e., self-study with

and without AVN-net) in a closed-book test after the same learning time to evaluate the usefulness of AVN-net. Both studies yielded promising results and confirmed that AVN-net can achieve expert-level performance in AVNFH diagnosis and provide effective support in clinical decision making and medical education.

The remainder of this paper is organized as follows. Section 2 reviews progress made in disease diagnosis and object detection with DL. Our primary contribution is also summarized in Section 2. Section 3 introduces all methods adopted in this study. Experimental results are discussed in Section 4. Section 5 describes the designs and results of pilot studies, followed by discussions in Section 6. Finally, conclusions are presented in Section 7.

II. RELATED WORK

A. Diagnosis with DL

Motivated by the significant success of DL, an increasing number of high-quality medical imaging datasets have been published, allowing researchers to thoroughly investigate the application of DL algorithms in different medical fields. For example, the ChestX-ray14 dataset [18], which comprises more than 110,000 chest X-ray images labeled with up to 14 diseases, supports thorax disease detection research using DL techniques. A series of studies have been conducted to drive the diagnostic performance of DL algorithms to the expert level [19], [20], [21], [22].

For musculoskeletal conditions, Rajpurkar *et al.* [23] proposed a DenseNet model [24] to detect upper extremity abnormalities based on a set of upper extremity radiographs. In a previous study [16], a VGG16-based model [25] was constructed to diagnose intertrochanteric hip fractures from proximal femoral radiographs, and the authors claimed their model exceeded the accuracy of orthopedic surgeons. However, the ROIs (i.e., proximal femurs) used to train the model were manually cropped from radiographs, which may hinder the potential application of the algorithm. To address this issue, Kazi *et al.* [26] employed the spatial transformation network architecture [27] to integrate tasks of the ROI localization and proximal femur fracture detection tasks into a single training process. Here, the diagnosis process can be automated, which broadens the scope of its potential application. However, as the ROIs were learned implicitly with the fracture detection training process, the performance and training efficiency of the entire model may not be optimal. Gale *et al.* [28] trained individual DCNN models using small subsets of data to achieve three preprocessing tasks, i.e., lateral-view detection, ROI localization, and metal detection. Thus, an individual model was constructed to focus on fracture diagnosis, and this model demonstrated state-of-the-art performance compared to previous methods.

In the AVNFH diagnosis context, Chee *et al.* [29] trained a ResNet-based model [30] for AVNFH detection from 1,800 AP view pelvic radiographs with corresponding MRI scans as a data annotation reference. To integrate findings from both MRI and radiographs, they applied the Association Research Circulation Osseous (ARCO) guideline [31] to differentiate

AVNFH stages. A noninferiority analysis was conducted, which confirmed that the performance of the DL algorithm is noninferior to that of radiologists. However, as the pathology of AVNFH stage I can only be observed from MRI, they did not clearly discuss how the MRI information was used. In addition, using only the AP view radiograph for AVNFH diagnosis is insufficient because subtle changes in the subchondral region may be missing owing to the overlapped anterior and posterior acetabular in the AP view [1], and all FHs were manually cropped from radiographs.

Differing from [29], in this study, we focus on radiographs from both AP and FL views to perform AVNFH diagnosis based on the Ficat staging system. Rather than training a single diagnosis algorithm, we developed an end-to-end system with state-of-the-art image classification and object detection algorithms to perform a series of subtasks automatically, which substantially enhances performance and utility. In addition, we performed studies to assess the utility of the proposed AVN-net in two real-world application scenarios.

B. Object detection with DL

Nowadays, DL-driven object detection algorithms are widely used in various applications, e.g., face recognition and security surveillance. Region-based CNNs (R-CNN) are a family of algorithms that represent a pioneering DL solution for object detection [32], [33], [34]. However, computational efficiency is always the most significant concern for R-CNNs because they perform a classification computation for all extracted regions, and the number of candidate regions for a single input image can be up to 2,000. Then, YOLO (i.e. You Only Look Once) model was proposed to address the low-efficiency problem by splitting the image into a grid [35]. However, it is inherently difficult to detect small objects due to the spatial constraint from image separation. To this end, the single-shot multi-box detector (SSD) model was designed to balance the speed and precision of object detection by performing classification on different feature scales [36]. As a result, the SSD model can detect bounding boxes of the target and perform classification in a single forward pass of the network.

III. METHODS

A. Data collection and annotation

All radiographs used in this study were extracted retrospectively from the radiology repository at Peking University Third Hospital, which is one of the largest tertiary referral hospitals in China. Radiographs from both AP and FL views of all AVNFH patients seen at the orthopedics clinic between 2005 and 2019 were included. We excluded radiographs with primary hip osteoarthritis, secondary osteoarthritis caused by developmental dysplasia of the hip, avascular necrosis with pathological fracture, and internal fixation remaining in the FH.

A panel of three orthopedic surgeons with at least 15 years of clinical and surgical experience was recruited for data annotation. When labeling FH bounding boxes, exam-views, and sides, each annotator was responsible for 1/3

of the data without overlapping. For AVNFH staging, the annotators individually labeled all FHs, and a list of typical cases for each stage was recorded. In addition, a short and categorical description of the reason/finding was provided by each annotator while supporting their annotation for each FH, e.g., cystic changes, FH deformation, and acetabular lesions for stages II, III, and IV, respectively. In case of disagreements, consensus discussion and majority voting were performed to obtain a final decision.

Because the pathological stage I cannot be observed on plain radiographs, we combined stages 0 and I as the AVNFH absence class. Thus, the classes for AVNFH staging included AVNFH absence, stage II, stage III, and stage IV. To facilitate performance evaluations, we further grouped stages II to IV as the AVNFH presence class. In addition, we defined stage II as the pre-collapse class and stage III combined with stage IV as the post-collapse class.

B. FH detection and postprocessing

Here, we adopted the SSD architecture [36], which performs object localization and classification in a single pass, to construct the FH detection model. To emphasize localization performance, we simplified the classification task using binary classes (i.e., FH vs non-FH). The training objective was to minimize multi-box loss, i.e., a weighted summation of the location loss based on the Intersection over Union (IoU) and confidence loss (i.e., the cross-entropy loss of the classification) [37]. The location loss (\mathcal{L}_{loc}), confidence loss (\mathcal{L}_{conf}), and multi-box loss (\mathcal{L}_{MB}) are expressed as follows:

$$\mathcal{L}_{loc}(x, l, g) = \frac{1}{2} \sum_{i,j} x_{i,j} \|l_i - g_j\|_2^2 \quad (1)$$

$$\begin{aligned} \mathcal{L}_{conf}(x, l, g) = & - \sum_{i,j} x_{i,j} \log c_i \\ & - \sum_{i,j} (1 - x_{i,j}) \log (1 - c_i) \end{aligned} \quad (2)$$

$$\mathcal{L}_{MB}(x, c, l, g) = \mathcal{L}_{conf}(x, l, g) + \alpha \mathcal{L}_{loc}(x, l, g) \quad (3)$$

where l_i is the i -th predicted boundary box coordinates, g_j is the j -th ground-truth coordinates, $x_{i,j} \in [0, 1]$ is the IoU between l_i and g_j , c_i is the confidence score for class i , and $\alpha = 1$ is the weight of the location loss.

With the detected boundary boxes, a postprocessing strategy was designed to augment the FH data. First, we adjusted the shape of the detected FH to be square by setting its side as the value of the longer edge of the original boundary box generated by the model while centering at the same position. Then, we introduced a scaling factor (denoted by s) and multiplied it to the side of FH square. Here, each detected FH area could be resampled with different scales by adjusting the s value. As a result, we could increase the size of the FH data used to train downstream modules by an order of magnitude.

C. Classifications

We defined exam-view and side identification, AVNFH diagnosis, and clinical note generation subtasks as individual

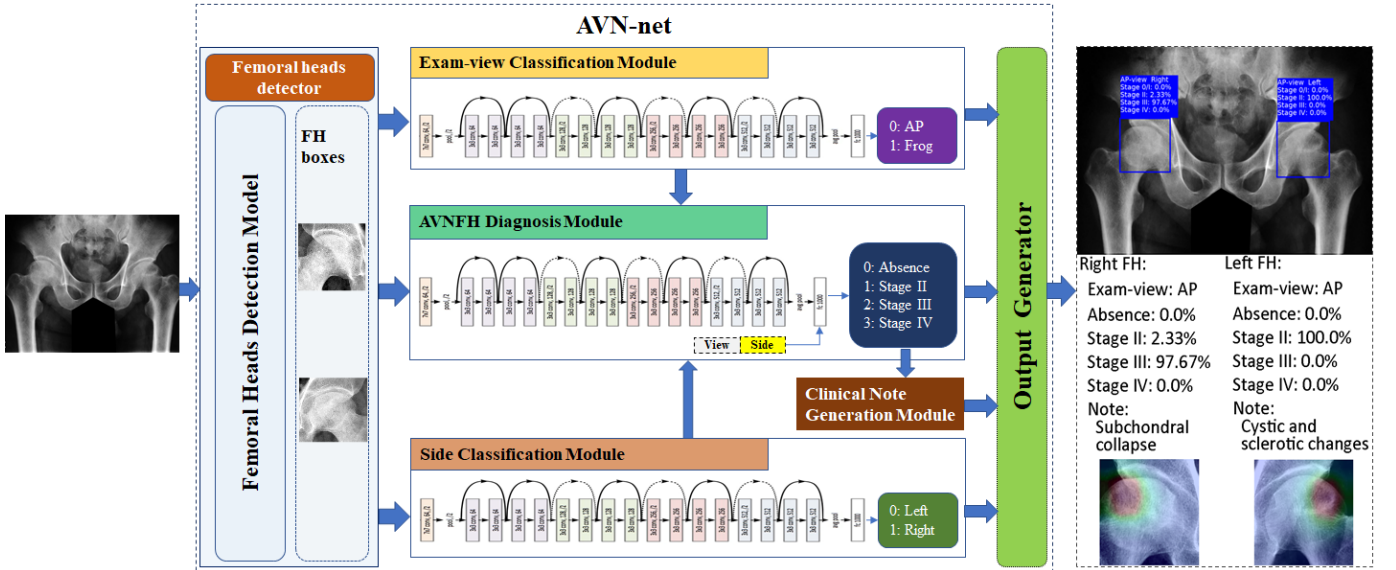


Fig. 2: System architecture of AVN-net. The FH detection module detects FH boundaries from the input radiograph and passes them to downstream modules. Both the exam-view and side classification modules are binary classifiers, and the AVN diagnosis and clinical note generation modules are multi-class/label classification tasks. The output generator integrates results from all upstream modules and outputs the visualized diagnosis.

classification problems based on the detected FHs. In consideration of the training efficiency, we uniformly adopted the 18-layer ResNet architecture to construct the backbone for each model. For the AVNFH diagnosis model, we initialized the weights with those of the well-trained exam-view classification model to facilitate the training process. Here, we combined non-image information (i.e., exam-views and sides generated by corresponding modules) with the feature map extracted by the DCNN as the input to the classification layer. The data size of each class was imbalanced; thus, we designed the loss function of the diagnosis model (\mathcal{L}_D) as a weighted summation of the cross-entropy loss and a Matthews correlation coefficient (MCC) regularization term. The MCC, which measures correlation between predicted and target values, is considered a stable metric of classifier performance with unbalanced data [38]. Formally, \mathcal{L}_D is defined as follows:

$$\mathcal{L}_D(x, y) = -\frac{1}{N} \sum_{i=1}^N y_i \log x_i + \beta \|1 - f_{mcc}(x_i, y_i)\|_2^2 \quad (4)$$

where x_i is the i -th predicted probability, y_i is the i -th label, $f_{mcc}(x_i, y_i)$ is the MCC between x_i and y_i , and β is a hyperparameter presenting the regularization weight.

Moreover, we framed clinical note generation as a multi-label classification problem based on the diagnosis results and categorical descriptions provided by the annotators. Specifically, we categorized the textual description from the annotators for each AVNFH stage into different classes and assigned each FH a multi-hot label. Then, we trained an individual classifier for each diagnosed stage to generate possible notes.

D. System architecture, models training and evaluation

Figure 2 shows the overall architecture of the proposed AVN-net. In AVN-net, the exam-view, side, diagnosis, and

clinical note generation modules take the FH data detected by the detection module as inputs. The output generator was constructed at the end of the workflow to integrate all intermediate results as the output.

When training the diagnosis model, we held the data of 50 randomly selected patients for testing. Here, 10-fold cross validation (CV) was performed to validate the performance, and the data splitting ratio at the patient level was set to 9:1 for the training and validation sets. For the remaining tasks, we split the FH data into training, validation, and test sets at a ratio of 70% : 10% : 20%. The initial learning rate for each task was set to 0.0001 and was halved when validation performance reached a plateau. In addition, we adopted the Adam optimizer with weight decay of 0.0005.

We assessed FH detection performance by measuring precision, recall, and F1, which are defined as follows.

$$Precision = \frac{True\ Positive}{True\ Positive + False\ Positive} \quad (5)$$

$$Recall = \frac{True\ Positive}{True\ Positive + False\ Negative} \quad (6)$$

$$F1 = 2 \cdot \frac{Precision \times Recall}{Precision + Recall} \quad (7)$$

The true positive (TP), false positive (FP), and false negative (FN) cases were determined by measuring IoU. Explicitly, for each ground truth FH box, we defined the detection as a TP case if the corresponding IoU was greater than a predefined threshold*. Otherwise, it was considered a FP. In addition, we counted the undetected FH as FN cases.

For classification models, we evaluated performance with AUC scores, sensitivity, specificity, and corresponding 95%

*In this paper, the IoU threshold is set to 0.5.

TABLE I: TESTING PERFORMANCE OF FH DETECTION MODEL WITH DIFFERENT IOU THRESHOLDS

| IoU threshold | Precision | Recall | F1 score |
|---------------|------------|---------------|---------------|
| 0.5 | 1.0 | 0.9721 | 0.9859 |
| 0.6 | 0.9806 | 0.9716 | 0.9761 |
| 0.7 | 0.9300 | 0.9701 | 0.9496 |
| 0.8 | 0.8068 | 0.9656 | 0.8791 |
| 0.9 | 0.7420 | 0.9628 | 0.8381 |

TABLE II: TESTING PERFORMANCE OF EXAM-VIEW, SIDE CLASSIFICATION, AND CLINICAL NOTE GENERATION MODELS

| Task | AUC (95% CI) | Sensitivity (95% CI) | Specificity (95% CI) |
|--------------------------|------------------------|------------------------|------------------------|
| Side | 0.9995 (0.9970-1.0) | 0.9965 (0.9805-1.0) | 0.9963 (0.9887-1.0) |
| Exam-view | 0.9997 (0.9975-1.0) | 0.9962 (0.9876-1.0) | 0.9965 (0.9908-1.0) |
| Clinical note generation | 0.9637 (0.9487-0.9743) | 0.8132 (0.8043-0.8428) | 0.9236 (0.9015-0.9431) |

confidence intervals (CIs) over the 10-fold CV. We tested the performance of the diagnosis model in three diagnostic tasks, i.e., AVNFB absences and presence detection, FH pre-/post-collapse classification (i.e., classifications of AVNFB absence, FH pre-collapse, and post-collapse), and AVNFB staging. In addition, we compared the performance of the best performing diagnosis model to that of four orthopedists with different experience levels on a new set of 100 typical AVNFB radiographs (50 AP view, 50 FL view). The participating orthopedists included two less-to-moderately experienced residents with average clinical experience of 3 years (denoted as group R), and two experienced attending surgeons with 7.5 years clinical experience on average (denoted as group S). Note that none of these orthopedists were involved in the data annotation process. The receiver operating characteristic (ROC) curves for each class were plotted, and time required for all readers to complete evaluations was recorded.

IV. RESULTS

A total of 3,136 radiographs (2,096 AP view and 1,040 FL view) from 841 patients were included in this study, including 5,089 FHs (absence: 1,025; stage II: 810; stage III: 1,271; stage IV: 1,983). In the FH detection modules postprocessing stage, we resampled each detected FH 10 times (15 times for typical cases) by linearly varying the scaling factor (s) value in the FH detection module from 0.9 to 1.0. As a result, a total of 56,935 FH images were obtained for the downstream classifications.

The FH detection model achieved precision, recall, and F1 scores of 1.0, 0.9721, and 0.9859, respectively, with the IoU threshold setting of 0.5. Table I lists the performance of the FH detection model with different IoU thresholds. The mean testing AUC of the side classification model over the 10-fold CV was 0.9995 (95% CI, 0.9970-1.0) with sensitivity and specificity of 0.9965 (95% CI, 0.9805-1.0) and 0.9963 (95% CI, 0.9887-1.0). The exam-view classifier obtained a

TABLE III: PERFORMANCE COMPARISON WITH STATE-OF-THE-ART RESULTS IN DIFFERENT TASKS

| Task and metrics | Proposed AVN-net | Chee <i>et al.</i> |
|---|----------------------------------|------------------------|
| AVNFB detection | | |
| Sensitivity (95% CI) | 0.8772 (0.8347-0.9348) | 0.848 (0.773-0.906) |
| Specificity (95% CI) | 0.9500 (0.9040-0.9710) | 0.913 (0.720-0.906) |
| FH pre-/post-collapse classification | | |
| Sensitivity of pre-collapse (95% CI) | 0.8896 (0.8144-0.9457) | 0.759 (0.624-0.865) |
| Sensitivity of post-collapse (95% CI) | 0.9324 (0.8629-0.9738) | 0.915 (0.825-0.965) |

TABLE IV: AVNFB STAGING PERFORMANCE ON TEST SET

| | Absence | Stage II | Stage III | Stage IV |
|-----------------------------|------------------------|------------------------|------------------------|------------------------|
| AUC (95% CI) | 0.9663 (0.9508-0.9789) | 0.9168 (0.8964-0.9415) | 0.8889 (0.8439-0.9232) | 0.9629 (0.9524-0.9721) |
| Sensitivity (95% CI) | 0.8382 (0.8004-0.8637) | 0.6941 (0.5444-0.7898) | 0.7491 (0.6546-0.8158) | 0.8930 (0.8759-0.9056) |
| Specificity (95% CI) | 0.9681 (0.9431-0.9864) | 0.9513 (0.9292-0.9663) | 0.8981 (0.8800-0.9243) | 0.9272 (0.9088-0.9433) |

mean testing AUC of 0.9997 (95% CI, 0.9975-1.0) with sensitivity of 0.9962 (95% CI, 0.9876-1.0) and specificity of 0.9965 (95% CI, 0.9908-1.0). For the clinical note generation task, the proposed model obtained a mean AUC of 0.9637 (95% CI, 0.9487-0.9803) with sensitivity of 0.8132 (95% CI, 0.8043-0.8428) and specificity of 0.9236 (95% CI, 0.9015-0.9431). The performance of side, exam-view, and clinical note classification modules is summarized in Table II.

In the AVNFB absence and presence detection task, the proposed AVN-net obtained a mean testing AUC of 0.9503 (95% CI, 0.9173-0.9774) with sensitivity of 0.8772 (95% CI, 0.8347-0.9348) and specificity of 0.9500 (95% CI, 0.9040-0.9710) over 10-fold CV. In the FH pre-/post-collapse classification task, AVN-net achieved a mean testing AUC of 0.9371 (95% CI, 0.9190-0.9500) with sensitivity of 0.8796 (95% CI, 0.8144-0.9457) and specificity of 0.8735 (95% CI, 0.8073-0.9317) for the pre-collapse classification, and a mean testing AUC of 0.9624 (95% CI, 0.9527-0.9719) with sensitivity of 0.9024 (95% CI, 0.8529-0.9538) and specificity of 0.9591 (95% CI, 0.9293-0.9844) for the post-collapse classification. Table III shows that the proposed AVN-net outperforms the state-of-art results in AVNFB detection and pre- and post-collapse classification tasks. For the AVNFB staging task, the proposed AVN-net obtained a mean testing AUC scores of 0.9663 (95% CI: 0.9508-0.9789), 0.9168 (95% CI: 0.8964-0.9415), 0.8889 (95% CI: 0.8439-0.9232), and 0.9629 (95% CI: 0.9524-0.9721) when identifying the AVNFB absence, Stage II, Stage III, and Stage IV classes, respectively. The detailed performance of the proposed model for the AVNFB staging task is given in Table IV.

When evaluating the performance of the proposed AVN-net against that of orthopedists on a new set of radiographs, AVN-net obtained sensitivity and specificity values of 0.9543 and 0.9231 in the AVNFB detection task. In contrast, the mean sensitivity and specificity for groups R and S were 0.8253

TABLE V: AVN-NET VS. ORTHOPEDISTS

| Tasks and Metrics | AVN-net | R1 ^a | R2 | S1 | S2 |
|---|-------------------------------|------------------------|------------------------|------------------------|-------------------------------|
| AVNFB detection | | | | | |
| F1 score (95% CI) | 0.9242 (0.8889-0.9646) | 0.8586 (0.8131-0.9091) | 0.8131 (0.7626-0.8687) | 0.9192 (0.8838-0.9596) | 0.9293 (0.8939-0.9646) |
| p-value ^b | – | p < 0.05 | p < 0.01 | p = 0.85 | p = 0.84 |
| FH pre-/post-collapse classification | | | | | |
| F1 score (95% CI) | 0.8586 (0.8131-0.9091) | 0.7576 (0.7020-0.8182) | 0.7172 (0.6566-0.7828) | 0.8636 (0.8182-0.9141) | 0.8939 (0.8535-0.9394) |
| p-value | – | p < 0.01 | p < 0.01 | p = 0.88 | p = 0.28 |
| AVNFB staging | | | | | |
| F1 score (95% CI) | 0.8232 (0.7727-0.8788) | 0.6263 (0.5606-0.6919) | 0.6361 (0.5704-0.7117) | 0.7768 (0.7273-0.8434) | 0.8131 (0.7626-0.8687) |
| p-value | – | p < 0.01 | p < 0.01 | p < 0.01 | p = 0.79 |

This table shows the performance and t-test results of AVN-net and orthopedists for different tasks with data of 10,000 bootstrap resampling.

^a R1 and R2 represent two less-to-moderately experienced residents; S1 and S2 represent two experienced surgeons.

^b T-test results of F1 scores between AVN-net and orthopedists.

and 0.8898, and 0.8601 and 0.9461, respectively. For the FH pre-collapse classification task, the sensitivity and specificity values were 0.8031 and 0.8943 for the proposed AVN-net, 0.5548 and 0.9120 for group R, and 0.7755 and 0.9627 for group S. For the post-collapse classification task, the sensitivity and specificity values obtained by the proposed AVN-net were 0.9143 and 0.9538, 0.9057 and 0.8821 for group R, and 0.9953 and 0.9576 for group S, respectively. For AVNFB staging, the sensitivity and specificity values obtained by the proposed AVN-net for the AVNFB absence, stage II, stage III, and stage IV classes were 0.9228 and 0.9189, 0.7041 and 0.9639, 0.7935 and 0.9531, 0.9678 and 0.9423, respectively. Here, group R obtained the mean sensitivity and specificity values of 0.8289 and 0.8889, 0.5573 and 0.9065, 0.5008 and 0.9029, and 0.9250 and 0.8594, respectively. Group S obtained the mean sensitivity and specificity values of 0.8684 and 0.9444, 0.7786 and 0.9604, 0.7459 and 0.9460, and 0.9257 and 0.9067, respectively. Figures 3a-3c show the ROC curves of the proposed AVN-net and the performance of orthopedists in the three diagnostic tasks, respectively. In addition, the mean time required to read each radiograph for groups R and S was 44.75 seconds (s) and 23.04 s, respectively.

In addition, we applied bootstrapping resampling with replacement to construct the 95% CI of F1 scores for the proposed AVN-net and orthopedists. We calculated the F1 of each model on the evaluation set and on 10,000 bootstrapping samples. Then, we took the 2.5th and 97.5th percentiles of the differences between the observed and bootstrapping F1 to estimate the distributions of F1 for each diagnosis task. Table V shows that the proposed AVN-net obtained a significantly higher ($p < 0.05$) F1 score than the less-to-moderately experienced orthopedists (group R) for all three diagnostic tasks and significantly better F1 ($p < 0.01$) than one experienced surgeon in the AVNFB staging task, while maintaining the same performance level as the experienced group for the remaining tasks.

V. PILOT STUDIES

To evaluate the utility of the proposed AVN-net, we conducted two pilot studies to investigate how well AVN-net helps orthopedists and medical students with diagnosis and self-study. To support these investigations, we developed a web application based on well-trained AVN-net models to allow users accessing the diagnosis of AVN-net.

A. AVN-net in diagnosis support: collaborative diagnosis

In this study, we invited the same group of orthopedists from the performance evaluation to stage a set of 30 new pelvic radiographs. Here, they were given all AVN-net results for reference when reading the radiographs, which included the diagnosis, class activation mappings [39] (which show the ROI for decision making), and the generated notes (e.g. the output of Fig. 2). Then, the diagnostic performance and time consumptions of each orthopedist were collected and compared to their previous records.

For group R, the mean sensitivity and specificity when diagnosing with AVN-net (without AVN-net) were 0.8750 and 0.9615 (0.8289 and 0.8889), 0.7813 and 0.9318 (0.5573 and 0.9065), 0.7787 and 0.9359 (0.5008 and 0.9029), 0.9000 and 0.9333 (0.9250 and 0.8594) for the AVNFB absence, stage II, stage III, and stage IV classes, respectively. For group S, the sensitivity and specificity values with AVN-net (without AVN-net) were 0.8750 and 0.9423 (0.8 and 0.9444), 0.8125 and 0.9545 (0.7786 and 0.9604), 0.7857 and 0.9487 (0.7459 and 0.9460), and 0.8777 and 0.9222 (0.9257 and 0.9067) for the AVNFB absence, stage II, stage III, and stage IV classes, respectively. Figure 3d shows the ROC curve of the proposed AVN-net when staging the new data and the performance of orthopedists with the AVN-net results for reference. The mean sensitivity of detecting stages II and III, which were difficult tasks for orthopedists in the evaluation phase, was improved by 48% and 5% for groups R and S, respectively, when collaboratively diagnosing using the proposed AVN-net.

We applied the same bootstrapping resampling strategy to construct the 95% CI of F1 scores for each orthopedist in the collaborative diagnosis. Table VI shows that, by referring to the "second opinion" from AVN-net, the F1 scores of all orthopedists were improved, and the improvements for both residents in group R and one surgeon in group S were statistically significant ($p < 0.01$). Regarding time consumption, group R spent an average of 11.45 s reading each radiograph with AVN-net (44.45 s without AVN-net), and group S spent 6.12 s on average (23.05 s without AVN-net), which were approximately four times faster than without AVN-net for both groups.

B. AVN-net in education assistance

In the field of medical education, learning from clinical experience plays an essential role in helping students as-

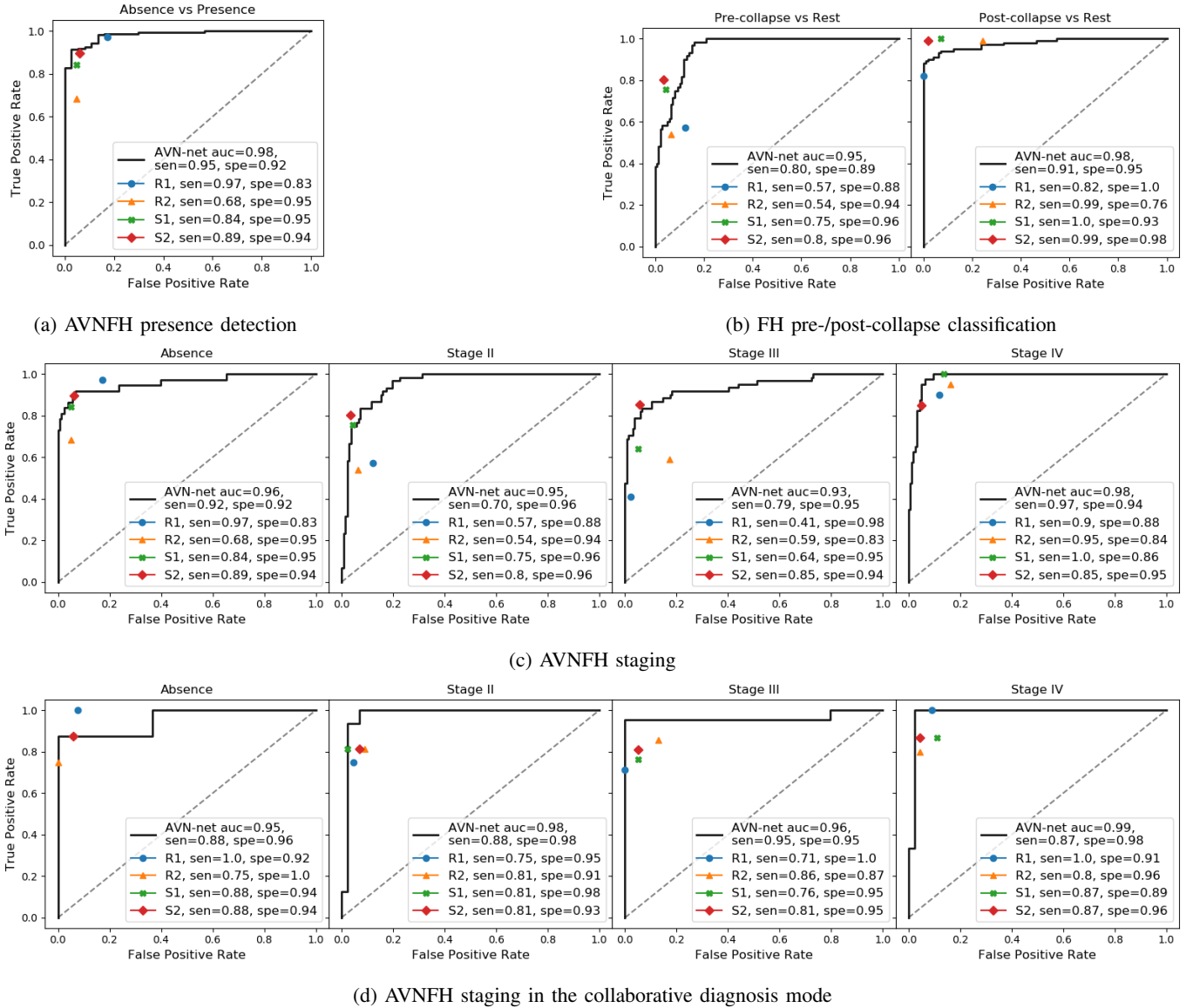


Fig. 3: Diagnostic performance in different tasks. (a) Performance of AVN-net and orthopedists in AVNFBH detection. (b) Performance of AVN-net and orthopedists in pre-/post-collapse classifications. (c) Performance of AVN-net and orthopedists in AVNFBH staging. (d) Performance of AVN-net and same group of orthopedists using the AVN-net results for reference on a set of 30 new pelvic radiographs. The auc, sen, and spe in legends represent AUC scores, sensitivity, and specificity, respectively.

simulate knowledge from books and develop practical skills. However, due to limited educational resources, it is unrealistic for students to receive constant guidance from domain experts. Consequently, the quality of self-study is critical to realize positive educational outcomes. Thus, we hypothesize that, in conjunction with knowledge learned from experienced experts, AVN-net can provide instructive and practical help to students in self-study than textbooks alone. Therefore, we recruited four senior medical students with similar academic performance and clinical experience to learn AVNFBH diagnosis in self-study to assess the effectiveness of the proposed AVN-net.

The students were randomly divided into control and experimental groups. A tutoring package (including 30 pelvic radiographs, the ground truth diagnosis, and a list of literature related to AVNFBH and the Ficat classification system) was

presented to both groups. Each group was allowed to obtain additional information (except for getting help from human experts). The control group was asked to learn AVNFBH staging with the given resources, and the experimental group was provided access to the AVN-net web application, with which they could observe the AVN-net diagnosis by uploading the provided examples or additional radiographs. After a two-hour learning period, we tested both groups with 30 new radiographs (60 FHs) in closed-book form. All radiographs selected for tutoring and testing were typical cases in corresponding stages. Here, the numbers of FHs in the test set for the AVNFBH absence, stage II, stage III, and stage IV categories were 14, 15, 17, and 14, respectively. The performance and time required by each student was also recorded and compared.

For the control group, the mean testing sensitivity and

TABLE VI: ORTHOPEDISTS COLLABORATING WITH AVN-NET

| Metrics | | R1 | R2 | S1 | S2 |
|---|--------------------------|---|----------------------------------|----------------------------------|----------------------------------|
| F1 (95% CI) | w/o ^a AVN-net | 0.6263 (0.5606-0.6919) | 0.6061 (0.5404-0.6717) | 0.7768 (0.7273-0.8434) | 0.8131 (0.7626-0.8687) |
| | w AVN-net | 0.8167 (0.7167-0.8833) p<0.01 ^b | 0.8333 (0.7333-0.9000) p<0.01 | 0.8175 (0.7246-0.9254) p<0.01 | 0.8333 (0.7413-0.9088) p=0.69 |
| Time^c (s/radiograph) | w/o AVN-net | 46.9 | 42.0 | 20.0 | 26.1 |
| | w AVN-net | 14.3 | 8.6 | 5.2 | 7.1 |

This table compares the F1 scores and time consumptions of each orthopedist with and without AVN-net results on the data of 10,000 bootstrapping samples.

^a w/o and w represent without and with the result of AVN-net for reference, respectively.

^b T-test results of F1 scores for each orthopedist with and without the results of AVN-net.

^c The mean time consumption for staging one radiograph.

TABLE VII: TESTING PERFORMANCE OF TWO GROUPS IN EDUCATION ASSISTANCE STUDY

| | Experimental group | Control group |
|-------------------------------|------------------------|------------------------|
| F1 score (95% CI) | 0.6750 (0.5833-0.7667) | 0.6167 (0.5333-0.7000) |
| p-value ^a | p<0.01 | - |
| Time (s/radiograph) | 70 | 75 |

^a T-test results of the F1 between experimental and control groups.

TABLE VIII: INTER-ORTHOPEDIST AGREEMENT IN AVNFB STAGING

| | Without AVN-net | | | | With AVN-net | | | |
|-----------------|-----------------|------|------|------|--------------|------|------|------|
| | R1 | R2 | S1 | S2 | R1 | R2 | S1 | S2 |
| R1 | 1 | 0.52 | 0.53 | 0.57 | 1 | 0.62 | 0.71 | 0.78 |
| R2 | - | 1 | 0.58 | 0.65 | - | 1 | 0.68 | 0.68 |
| S1 | - | - | 1 | 0.69 | - | - | 1 | 0.75 |
| GT ^a | 0.56 | 0.55 | 0.71 | 0.79 | 0.78 | 0.72 | 0.75 | 0.77 |

This table lists Cohen's Kappa statistics between each pair of orthopedists in ordinary and collaborative diagnosis modes.

^a GT represents ground truth labels.

specificity for detecting AVNFB absence, stage II, stage III, stage IV were 0.4286 and 0.9457, 0.7333 and 0.8000, 0.6471 and 0.8488, and 0.6429 and 0.8913, respectively. For the experimental group, these values were 0.6071 and 0.9674, 0.7333 and 0.8222, 0.6765 and 0.6372, and 0.6786 and 0.9348 for each category, respectively. We constructed the 95% CI of F1 scores for both groups using the same bootstrapping strategy. Table VII shows that the experimental group obtained a mean testing F1 score of 0.6750 (95% CI, 0.5833-0.7667), which was significantly greater ($p < 0.01$) than that of the control group (0.6167, 95% CI: 0.5333-0.7000). The mean time consumption for the experimental group was slightly less than that of the control group (70 vs 75 s/radiograph).

VI. DISCUSSION

As the first diagnostic imaging modality for AVNFB, it would be extremely beneficial for patient care if detect early-stage AVNFB from the radiograph in a timely manner. However, due to the modest changes between the stages of AVNFB, accurate diagnosis from a plain radiograph is a significant

challenge, especially for relatively less experienced clinicians, which results in poor diagnostic consistency.

In the evaluation phase, we confirmed that the proposed AVN-net is able to obtain state-of-the-art performance in AVNFB diagnosis and significantly outperforms less-to-moderately experienced orthopedists, which allows us to further investigate the utility of AVN-net. Thus, in a subsequent collaborative diagnosis study, we found that all participants could obtain the same level of diagnostic performance as the experienced orthopedist when conducting diagnosis using AVN-net, and the time required to examine each radiograph was reduced by a factor of four. Figure 4 shows the confusion matrices of orthopedists and AVN-net in collaborative diagnosis, where G/P in the label of each row/column represents the ground truth/prediction, Ab, S2, S3, and S4 represent the absence, stage II, stage III, and stage IV classes, and the number in each cell is the number of predictions for the corresponding category. As can be seen, the proposed AVN-net consistently facilitated high-quality performance in tasks that were difficult for orthopedists. Thus, AVN-net, which provides orthopedists with reliable and complementary diagnostic support, is considered a valuable tool for clinicians relative to efficiently eliminating noise and making decisions.

To further understand the influence of AVN-net on diagnostic consistency, we compared Cohen's Kappa statistics [40] between each orthopedist in AVNFB staging with and without AVN-net classes for reference. Table VIII shows that, when collaborating with AVN-net, the intra-group diagnosis agreements for groups R and S (i.e., the Kappa between readers in the same group) increased by 19.2% and 8.7%, respectively, and the inter-group agreement (i.e., the mean Kappa between the groups R and S) was improved by over 22.4% (from 0.58 to 0.71). In addition, agreement between group R and the ground truth increased by 35.1% (from 0.555 to 0.75) when collaborating with AVN-net and the value for group S was maintained at the same level (0.75 vs 0.76). Therefore, we are confident that the second opinion provided by the proposed AVN-net was beneficial to all orthopedists and enhanced diagnostic performance and consistency, and the proposed AVN-net is especially valuable for less-to-moderately experienced orthopedists in diagnostic decision making. Furthermore, when looking at cases that AVN-net misclassified, we found that, for each misclassified example,

| | R1 | | | | R2 | | | | S1 | | | | S2 | | | | AVN-net | | | |
|------|------|------|------|------|------|------|------|------|------|------|------|------|------|------|------|------|---------|------|------|------|
| G-Ab | 8 | 0 | 0 | 0 | 6 | 2 | 0 | 0 | 7 | 1 | 0 | 0 | 7 | 1 | 0 | 0 | 7 | 1 | 0 | 0 |
| G-S2 | 4 | 12 | 0 | 0 | 0 | 13 | 3 | 0 | 3 | 13 | 0 | 0 | 3 | 13 | 0 | 0 | 2 | 14 | 0 | 0 |
| G-S3 | 0 | 2 | 15 | 4 | 0 | 1 | 18 | 2 | 0 | 0 | 16 | 5 | 0 | 2 | 17 | 2 | 0 | 0 | 20 | 1 |
| G-S4 | 0 | 0 | 0 | 15 | 0 | 1 | 2 | 12 | 0 | 0 | 2 | 13 | 0 | 0 | 2 | 13 | 0 | 0 | 2 | 13 |
| | P-Ab | P-S2 | P-S3 | P-S4 | P-Ab | P-S2 | P-S3 | P-S4 | P-Ab | P-S2 | P-S3 | P-S4 | P-Ab | P-S2 | P-S3 | P-S4 | P-Ab | P-S2 | P-S3 | P-S4 |

Fig. 4: Classification results of orthopedists in the collaborative diagnosis

| | Orthopedists | | | | Students | | | |
|------|--------------|------|------|------|----------|------|------|------|
| G-Ab | 129 | 19 | 4 | 0 | 29 | 27 | 0 | 0 |
| G-S2 | 52 | 163 | 27 | 2 | 8 | 44 | 8 | 0 |
| G-S3 | 2 | 17 | 152 | 73 | 0 | 7 | 45 | 16 |
| G-S4 | 0 | 1 | 11 | 148 | 0 | 0 | 19 | 37 |
| | P-Ab | P-S2 | P-S3 | P-S4 | P-Ab | P-S2 | P-S3 | P-S4 |

Fig. 5: Confusion matrices of all orthopedists and students in the task of AVNFB staging without the presence of AVN-net

at least one orthopedist was able to make a correct diagnosis using AVN-net’s suggestion, which, to some extent, proves that AVN-net’s second opinion cannot place human assessment.

We also obtained a promising result from the medical education study. The group of students who were self-learning AVNFB diagnosis using AVN-net achieved significantly better test performance and spent slightly less time on average than the group of students that did not use AVN-net. In addition, we found that both groups obtained similar or even better testing performance (F1 score) than the less experienced orthopedists. We think this could have resulted from the different number of radiographs and time spent on staging each radiograph, which also implies two possible causes of poor inter-reader agreement. Interestingly, when comparing the confusion matrices of all students with orthopedists for the AVNFB staging task, we found some distinct performance patterns (Fig. 5). Specifically, the students were more sensitive to identifying AVNFB stages II and III, which were difficult for the orthopedists (especially for the less-to-moderately experienced group). In contrast, the orthopedists achieved much higher accuracy in detecting extreme categories (i.e., AVNFB absence and stage IV) than the students. We suspect this can be attributed to the different clinical experience between the readers, which suggests that we should design different strategies for various applications.

Due to a data limitation, we defined the clinical note generate task in the diagnosis module as a classification problem based on categorical descriptions provided by the experts,

which could potentially impact explainability. We believe that textual information would play a critical role relative to improving model training performance and providing more informative hints. Thus, we plan to use diagnosis reports from radiographs as an additional data dimension in future. In addition, we solely focused on AVNFB diagnosis from plain radiographs and AVNFB stage I is not visible in X-ray images; thus, the capability of early-stage detection with the proposed system may be constrained. Therefore, in future, we also plan to extend the scope of this study by involving MRI data and subdivisions in each stage based on the ARCO system.

VII. CONCLUSION

In this paper, we have presented an automated AVNFB diagnosis system based on DL algorithms and plain radiographs of the pelvis (AVN-net). The proposed AVN-net demonstrated state-of-the-art performance in various diagnostic tasks and significantly outperformed the less-to-moderately experienced orthopedists while maintaining same performance level of experienced orthopedists.

In addition, we conducted two pilot studies to investigate the utility of the proposed AVN-net, where AVN-net was used for diagnosis support and education assistance. The results of both studies confirm that AVN-net, which was trained using knowledge from domain experts, is especially helpful for less-to-moderately experienced orthopedic practitioners, e.g., residents and students, in making diagnostic decisions.

In conclusion, the proposed AVN-net achieved expert-level performance in AVNFB diagnosis and provides efficient and effective support in both clinical decision-making and medical education

REFERENCES

- [1] M. A. Mont and D. S. Hungerford, “Non-traumatic avascular necrosis of the femoral head.” *J. Bone Joint Surg.*, vol. 77, no. 3, pp. 459–474, 1995.
- [2] D. Petek, D. Hannouche, and D. Suva, “Osteonecrosis of the femoral head: pathophysiology and current concepts of treatment,” *EFORT Open Rev.*, vol. 4, no. 3, pp. 85–97, 2019.
- [3] J. Moya-Angeler, A. L. Gianakos, J. C. Villa, A. Ni, and J. M. Lane, “Current concepts on osteonecrosis of the femoral head,” *World J. Orthop.*, vol. 6, no. 8, p. 590, 2015.

- [4] W. G. BOETTCHER, M. BONFIGLIO, H. H. HAMILTON, R. F. SHEETS, and K. SMITH, "Non-traumatic necrosis of the femoral head: Part 1. relation of altered hemostasis to etiology," *J. Bone Joint Surg.*, vol. 52, no. 2, pp. 312–321, 1970.
- [5] R. K. Sen, "Management of avascular necrosis of femoral head at pre-collapse stage," *Indian J. Orthop.*, vol. 43, no. 1, p. 6, 2009.
- [6] P. Hernigou, A. Poignard, A. Nogier, and O. Manicom, "Fate of very small asymptomatic stage-i osteonecrotic lesions of the hip," *J. Bone Joint Surg.*, vol. 86, no. 12, pp. 2589–2593, 2004.
- [7] J. K. Bradway and B. F. Morrey, "The natural history of the silent hip in bilateral atraumatic osteonecrosis," *J. Arthrop.*, vol. 8, no. 4, pp. 383–387, 1993.
- [8] H. E. Jergesen and A. S. Khan, "The natural history of untreated asymptomatic hips in patients who have non-traumatic osteonecrosis," *J. Bone Joint Surg.*, vol. 79, no. 3, pp. 359–63, 1997.
- [9] R. Ficat, "Idiopathic bone necrosis of the femoral head. early diagnosis and treatment," *J. Bone Joint Surg. Br. Volume*, vol. 67, no. 1, pp. 3–9, 1985.
- [10] Z. Stoica, D. Dumitrescu, M. Popescu, I. Gheonea, M. Gabor, and N. Bogdan, "Imaging of avascular necrosis of femoral head: familiar methods and newer trends," *Curr. Health Sci. J.*, vol. 35, no. 1, p. 23, 2009.
- [11] R. M. Kay, J. R. Lieberman, F. J. Dorey, and L. L. Seeger, "Interobserver and intraobserver variation in staging patients with proven avascular necrosis of the hip," 1994.
- [12] V. Gulshan, L. Peng, M. Coram, M. C. Stumpe, D. Wu, A. Narayanaswamy, S. Venugopalan, K. Widner, T. Madams, J. Cuadros *et al.*, "Development and validation of a deep learning algorithm for detection of diabetic retinopathy in retinal fundus photographs," *JAMA*, vol. 316, no. 22, pp. 2402–2410, 2016.
- [13] Z. Li, Y. He, S. Keel, W. Meng, R. T. Chang, and M. He, "Efficacy of a deep learning system for detecting glaucomatous optic neuropathy based on color fundus photographs," *Ophthalmology*, vol. 125, no. 8, pp. 1199–1206, 2018.
- [14] A. Esteva, B. Kuprel, R. A. Novoa, J. Ko, S. M. Swetter, H. M. Blau, and S. Thrun, "Dermatologist-level classification of skin cancer with deep neural networks," *Nature*, vol. 542, no. 7639, p. 115, 2017.
- [15] H. A. Haenssle, C. Fink, R. Schneiderbauer, F. Toberer, T. Buhl, A. Blum, A. Kallou, A. B. H. Hassen, L. Thomas, A. Enk *et al.*, "Man against machine: diagnostic performance of a deep learning convolutional neural network for dermoscopic melanoma recognition in comparison to 58 dermatologists," *Ann. Oncol.*, vol. 29, no. 8, pp. 1836–1842, 2018.
- [16] T. Urakawa, Y. Tanaka, S. Goto, H. Matsuzawa, K. Watanabe, and N. Endo, "Detecting intertrochanteric hip fractures with orthopedist-level accuracy using a deep convolutional neural network," *Skeletal Radiol.*, vol. 48, no. 2, pp. 239–244, 2019.
- [17] S. W. Chung, S. S. Han, J. W. Lee, K.-S. Oh, N. R. Kim, J. P. Yoon, J. Y. Kim, S. H. Moon, J. Kwon, H.-J. Lee *et al.*, "Automated detection and classification of the proximal humerus fracture by using deep learning algorithm," *Acta Orthop.*, vol. 89, no. 4, pp. 468–473, 2018.
- [18] X. Wang, Y. Peng, L. Lu, Z. Lu, M. Bagheri, and R. M. Summers, "Chestx-ray8: Hospital-scale chest x-ray database and benchmarks on weakly-supervised classification and localization of common thorax diseases," in *Proc. IEEE Conf. on Computer Vision and Pattern Recognition*, 2017, pp. 2097–2106.
- [19] L. Yao, E. Poblens, D. Dagunts, B. Covington, D. Bernard, and K. Lyman, "Learning to diagnose from scratch by exploiting dependencies among labels," *arXiv Preprint ArXiv:1710.10501*, 2017.
- [20] P. Rajpurkar, J. Irvin, K. Zhu, B. Yang, H. Mehta, T. Duan, D. Ding, A. Bagul, C. Langlotz, K. Shpanskaya *et al.*, "Chexnet: Radiologist-level pneumonia detection on chest x-rays with deep learning," *arXiv preprint arXiv:1711.05225*, 2017.
- [21] P. Rajpurkar, J. Irvin, R. L. Ball, K. Zhu, B. Yang, H. Mehta, T. Duan, D. Ding, A. Bagul, C. P. Langlotz *et al.*, "Deep learning for chest radiograph diagnosis: A retrospective comparison of the chexnext algorithm to practicing radiologists," *PLOS Med.*, vol. 15, no. 11, p. e1002686, 2018.
- [22] Q. Guan, Y. Huang, Z. Zhong, Z. Zheng, L. Zheng, and Y. Yang, "Diagnose like a radiologist: Attention guided convolutional neural network for thorax disease classification," *arXiv Preprint ArXiv:1801.09927*, 2018.
- [23] P. Rajpurkar, J. Irvin, A. Bagul, D. Ding, T. Duan, H. Mehta, B. Yang, K. Zhu, D. Laird, R. L. Ball *et al.*, "Mura: Large dataset for abnormality detection in musculoskeletal radiographs," *arXiv Preprint ArXiv:1712.06957*, 2017.
- [24] G. Huang, Z. Liu, K. Q. Weinberger, and L. van der Maaten, "Densely connected convolutional networks," in *Proc. IEEE Conf. on Computer Vision and Pattern Recognition*, vol. 1, no. 2, 2017, p. 3.
- [25] K. Simonyan and A. Zisserman, "Very deep convolutional networks for large-scale image recognition," *arXiv Preprint ArXiv:1409.1556*, 2014.
- [26] A. Kazi, S. Albarqouni, A. J. Sanchez, S. Kirchoff, P. Biberthaler, N. Navab, and D. Mateus, "Automatic classification of proximal femur fractures based on attention models," in *Intl. Workshop on Mach. Learn. in Med. Imaging*. Springer, 2017, pp. 70–78.
- [27] M. Jaderberg, K. Simonyan, A. Zisserman *et al.*, "Spatial transformer networks," in *Adv. Neural Inf. Process. Syst.*, 2015, pp. 2017–2025.
- [28] W. Gale, L. Oakden-Rayner, G. Carneiro, A. P. Bradley, and L. J. Palmer, "Detecting hip fractures with radiologist-level performance using deep neural networks," *arXiv Preprint ArXiv:1711.06504*, 2017.
- [29] C. G. Chee, Y. Kim, Y. Kang, K. J. Lee, H.-D. Chae, J. Cho, C.-M. Nam, D. Choi, E. Lee, J. W. Lee *et al.*, "Performance of a deep learning algorithm in detecting osteonecrosis of the femoral head on digital radiography: A comparison with assessments by radiologists," *Am. J. Roentgenol.*, pp. 1–8.
- [30] K. He, X. Zhang, S. Ren, and J. Sun, "Deep residual learning for image recognition," in *Proc. IEEE Conf. on Computer Vision and Pattern Recognition*, 2016, pp. 770–778.
- [31] J. Gardniers, "Arco committee on terminology and staging (report on the committee meeting at santiago de compostela)," *ARCO Newsl.*, vol. 5, pp. 79–82, 1993.
- [32] R. Girshick, J. Donahue, T. Darrell, and J. Malik, "Rich feature hierarchies for accurate object detection and semantic segmentation," in *Proc. IEEE Conf. on Computer Vision and Pattern Recognition*, 2014, pp. 580–587.
- [33] R. Girshick, "Fast r-cnn," in *Proc. IEEE Intl. Conf. on Computer Vision*, 2015, pp. 1440–1448.
- [34] S. Ren, K. He, R. Girshick, and J. Sun, "Faster r-cnn: Towards real-time object detection with region proposal networks," in *Adv. Neural Inf. Process. Syst.*, 2015, pp. 91–99.
- [35] J. Redmon, S. Divvala, R. Girshick, and A. Farhadi, "You only look once: Unified, real-time object detection," in *Proc. IEEE Conf. on Computer Vision and Pattern Recognition*, 2016, pp. 779–788.
- [36] W. Liu, D. Anguelov, D. Erhan, C. Szegedy, S. Reed, C.-Y. Fu, and A. C. Berg, "Ssd: Single shot multibox detector," in *Lecture Notes in Computer Science European Conf. on Computer Vision*. Springer, 2016, pp. 21–37.
- [37] C. Szegedy, S. Reed, D. Erhan, D. Anguelov, and S. Ioffe, "Scalable, high-quality object detection," *arXiv Preprint ArXiv:1412.1441*, 2014.
- [38] J. Gorodkin, "Comparing two k-category assignments by a k-category correlation coefficient," *Comp. Biol. Chem.*, vol. 28, no. 5-6, pp. 367–374, 2004.
- [39] B. Zhou, A. Khosla, A. Lapedriza, A. Oliva, and A. Torralba, "Learning deep features for discriminative localization," in *Proc. IEEE Conf. on Computer Vision and Pattern Recognition*, 2016, pp. 2921–2929.
- [40] J. Cohen, "A coefficient of agreement for nominal scales," *Educ. Psychol. Meas.*, vol. 20, no. 1, pp. 37–46, 1960.